Science Advances
AAAS

Supplementary Materials for

Conformability of flexible sheets on spherical surfaces

Siyi Liu *et al.*

Corresponding author: Nanshu Lu, nanshulu@utexas.edu; Ying Li, yli2562@wisc.edu

Sci. Adv. **9**, eadf2709 (2023)
DOI: 10.1126/sciadv.adf2709

The PDF file includes:

Supplementary Text
Figs. S1 to S9
Tables S1 to S4
Legends for movies S1 to S3

Other Supplementary Material for this manuscript includes the following:

Movies S1 to S3

1. Curved Design of the Cut

For cut-facilitated design, the cut opening can be nonlinear for better coverage on the target substrate. The cut opening can be estimated by pure geometric relations. Assuming no radial stretching applied on the thin sheet, the entire sheet is subjected to hoop compression, which is a function of the radial coordinate r. Equation (9) offers the total hoop compression

$$\Delta(r) = 2\pi\left(r - \rho \sin\frac{r}{\rho}\right) \tag{S1}$$

If the cut is a simple parallel narrow slit, such a compression induces sheet overlapping instead of buckle delamination, as shown in **Fig. S3**. Here, we propose a curved design to achieve a high coverage without overlapping by considering the hoop compression in Eq. (S1). Assuming M cuts of length l are made to improve the conformability of a sheet of radius $R > r_c$, we can obtain the slit opening, *i.e.*, the material to be removed at each cut is

$$w(r) = \frac{\Delta(r)}{M} = \frac{2\pi\left(r-\rho \sin\frac{r}{\rho}\right)}{M} \tag{S2}$$

Using the 90% conformability strategy Eq. (16), the cut opening can be obtained

$$w(r) = \begin{cases} 0 & r < r_c \\ 0.73\pi L_{\mathrm{ec}} \frac{r-\rho \sin\frac{r}{\rho}}{R-r_c} & r > r_c \end{cases} \tag{S3}$$

It indicates that the cut starts at $r = r_c$ and is curved as shown in **Fig. 6C**. Simulation is performed to validate this design for a sheet with a radius of 15 mm conformed to a spherical surface of a radius of 30 mm, as shown in **Fig. 6C**. The thin sheet has 12 curved slits of 12.9 mm long. It conformed well to the spherical substrate, and its conformability is 96% without any overlapping. **Movie S3** shows the entire conforming process and final morphology in simulation.

2. Model Calibration and Reduced-Scale Structural Model

For thin-sheet structures, on the macroscopic scale, finite element methods usually have difficulties in separating the contribution of different deformation types, e.g., stretching and bending. Hence, molecular dynamics (MD) simulations are more suitable to model the water-assisted transfer process. However, using MD simulations at a

microscopic scale can be time-consuming and costly due to the large number of atoms and the small timestep for integration. To overcome these challenges, the experimental setup was first scaled to the atomic scale, and then a particle-based coarse-grained approach was employed to model the deformable sheet at the atomic scale in this work. Following coarse-grained molecular dynamics (CGMD), one particle can represent a part of the scaled sheet to reduce the degrees of freedom in the system. The mechanical properties in both simulation and physical space are listed in **Table S1**.

Table S1 Material parameters used in CGMD and their corresponding physical values

Parameters	Simulation	Physical
Length scale	1	1×10^{-4} m
Force scale	1	1.70×10^{-3} N
Surface tension	3.970×10^{-3}	7.200×10^{-2} N m^{-1}
Adhesion energy	7.940×10^{-3}	1.440×10^{-1} N m^{-1}
Stretching constant	1500	2.546×10^{4} N m^{-1}
Bending constant	4.313	7.171×10^{-7} N m

Since the unit system in simulation (e.g., time, temperature, amount of substance, length, etc.) is totally different from the physical values in the experiments, a calibration of the material parameters is required. Three key material properties, the sheet bending rigidity, stretching stiffness, and adhesion energy, must be correctly converted in the simulation because they are governing the buckling delaminations. The material parameters in our simulation were calibrated based on a top-down method to achieve experimental observations by a trial-and-error heuristic search in CGMD.

We first determine the length scaling factor: 1 mm in the experiment corresponds to 10 in the simulation. Taking the case of ρ = 50 mm and R = 5 mm in the experiment as an example, in the simulation, 500 was calculated to be the scaled radius of the substrate, and the scaled radius of the sheet was calculated to be 50. In the simulation, we selected the average distances of the discretized particles (the mesh size) in the sheet and substrate to be 2 and 1.5, respectively. The equilibrium distance σ between sheet particles was set to be 2, at which the potential energy between the sheet particles was zero, while the cutoff was set to be 2σ.

We then find an initial combination of the sheet bending rigidity, stretching stiffness, and adhesion energy as a starting point for our parameter calibration. The stretching coefficient (k_{s}) and bending coefficient (k_{bend}) were first calculated based on the Helfrich model. [47, 48] In the Helfrich model, $k_{\mathrm{s}} = \frac{Eh}{3^{0.5}(1-\nu^2)}$, and $k_{\mathrm{b}} = \frac{2Eh^3}{12\times 3^{0.5}(1-\nu^2)}$, where E is Young's modulus, h is thickness, and ν is the Poisson ratio. The potential well depth (ε) between substrate and sheet particles in the CGMD model governs the interfacial adhesion. To calculate the potential well depth, a sheet with a radius of 5 mm was placed at a distance σ above a square plate with a side length of 15 mm, as shown in **Fig. S7**. The adhesion energy was the total potential between the sheet particles and the substrate particles in the CGMD model. We then obtained an initial ε, and eventually, we found ε = 0.16 offered the adhesion energy per unit area of 0.144 J m^{-2}. Note that if the mesh size changes, the potential well depth must be recalibrated. However, this set of material properties was not the correct material parameters in simulation space since other units affected the unit conversion for the force unit. Therefore, it is essential to find the correct unit conversion for the forces.

After that, we performed a trial-and-error heuristic search to find the correct combination of k_{s}, k_{b}, and ε simultaneously employed them as material parameters. The correct property must achieve approximately the same sheet edge deflection, buckling number, and sheet conformability as the experiments. We performed this search based on two cases, sheets with radii of 5 mm and 7 mm on the substrate with a radius of 50 mm, as shown in **Fig. 3** and **Fig. S1.** The three macroscopic behaviors of both cases by CGMD simulation agreed well with their corresponding experimental results. Based on the physical parameter shown in Table S1, the calibrated stretching coefficient k_{s} and bending coefficient k_{bend} were 1500 and 4.313 for the lattice-spring model, respectively. The potential well depth (ε) between the substrates and the sheet particles is determined by adhesion energy per unit, as shown in **Fig. S8.** The equilibrium distance σ between the substrate and the sheet particle was set to be 0.2 mm. These calibrated parameters were used in all other cases. To demonstrate the validity of this combination of material parameters in simulation, the normalized maximum radius of complete contact $\bar{r} =$ c

$1.9(\gamma/Eh)^{1/4}$ can be calculated to be 0.068 in simulation and 0.070 in physical experiments. The error came from the adhesion energy calculation in simulation but is reasonably small.

In addition, the size scaling and top-down method will take two scaling factors: the length scaling factor, C_{length} and the force scaling factor, C_{force}. The length scaling factor can be written as $C_{\text{length}} = \frac{L_{\text{simulation}}}{L_{\text{physical}}} = 1 \times 10^4\ \text{m}^{-1}$, where $L_{\text{simulation}}$ and L_{physical} are the unit length in the simulation and physical space, respectively. The force scaling factor can be expressed as $C_{\text{force}} = \frac{F_{\text{simulation}}}{F_{\text{physical}}} = 5.88 \times 10^{-4}\ \text{N}^{-1}$, where $F_{\text{simulation}}$ and F_{physical} are the unit force in the simulation and physical space, respectively. Finally, based on the two scaling factors, the results from the simulation scale can be transformed into the experimental scale. In this work, we consider three types of substrate radii and a wide range of different sheet radii as listed in **Table S2**.

Table S2 Geometric parameters of substrate and sheet simulated by CGMD

Simulation		Physical (mm)		Sheet radius-to-substrate radius ratio
Substrate radius	Sheet radius	Substrate radius	Sheet radius	
300	30.0	30	3.0	0.10
	40.0		4.0	0.13
	50.0		5.0	0.17
	60.0		6.0	0.20
	70.0		7.0	0.23
	80.0		8.0	0.27
	90.0		9.0	0.30
	100.0		10.0	0.33
500	35.0	50	3.5	0.07
	50.0		5.0	0.10
	70.0		7.0	0.14
	100.0		10.0	0.20
	120.0		12.0	0.24
	140.0		14.0	0.28
700	35.0	70	3.5	0.05

	70.0		7.0	0.07
	90.0		9.0	0.10
	100.0		10.0	0.14
	120.0		12.0	0.17
	140.0		14.0	0.20

Besides, we studied the effect of the mesh size. In the above simulations, the distance of the discretized particles in the sheets (the mesh size) was selected to be 2 based on previous experiences. To study how the mesh size affects the sheet buckling, we took a sheet with a radius of 5 mm and a substrate with a radius of 50 mm as an example (Corresponding to a sheet with a radius of 50 and a substrate with a radius of 500 in simulations, and see simulation parameters in **Table S3** for details). We simulated the sheets conforming to the spherical substrates with four different mesh sizes, 0.5, 1, 2, and 4. We first calibrated the potential well depth ε and plotted it as a function of the mesh size, as shown in **Fig. S9A**. Then, five independent models were simulated for the same sheet and substrate radius. Their conformability is plotted in **Fig. S9B,** and their edge deflections are plotted in **Fig. S9C**. It can be observed that the mesh size does not play a significant role in these macroscopic buckling behaviors. Therefore, we choose 2.0 as the mesh size for all the following studies.

Table S3 The model parameters for the thin sheet with different mesh sizes

Mesh size	Particle number	Particle mass	Epsilon	Sigma	Cut off
0.5	32866	0.0258	0.010	2.0	4.0
1	8424	0.1007	0.028	2.0	4.0
2	2151	0.3945	0.085	2.0	4.0
4	610	1.3912	0.230	2.0	4.0

3. Computational Method for Cut-Facilitated Design

For cut-facilitated design, we first simulated the experiments using the above calibrated potential parameters to validate our simulation. Taking the sheet with a radius of 7 mm and the substrate with a radius of 50 mm as an example, we simulated l= 2 mm

and M = 3, l = 3 mm and M = 2, and l = 3 mm and M = 3 to compare their sheet conformability, contour plots of the gap between the sheet and the substrate, and the gap between the sheet and the substrate along the boundary of the circular sheet. In simulations, the sheet radius is 70 and the substrate radius is 500. The cut length l = 2 mm and 3 mm corresponds to l = 20 and 30, respectively.

After validation, to study how the cut-facilitated design affects the sheet conformability, we consider different cut lengths and cut numbers for a sheet with a radius of 10 mm on a substrate with a radius of 30 mm (Corresponding to a sheet with a radius of 100 and a substrate with a radius of 300 in simulations). **Table S4** lists the cut length and cut number we investigated by simulation. The mesh size of 2.0 is used in all CGMD simulations. Their conformability is calculated and plotted in **Fig. 6C.**

Table S4 Different combinations of cut length and cut number

The substrate with a radius of 300 and the thin sheet with a radius of 100						
Cut length l	Cut number M					
10	2	3	4	6	8	10
30	2	3	4	6	8	10
50	2	3	4	6	8	10
70	2	3	4	6	8	10
90	2	3	4	6	8	10

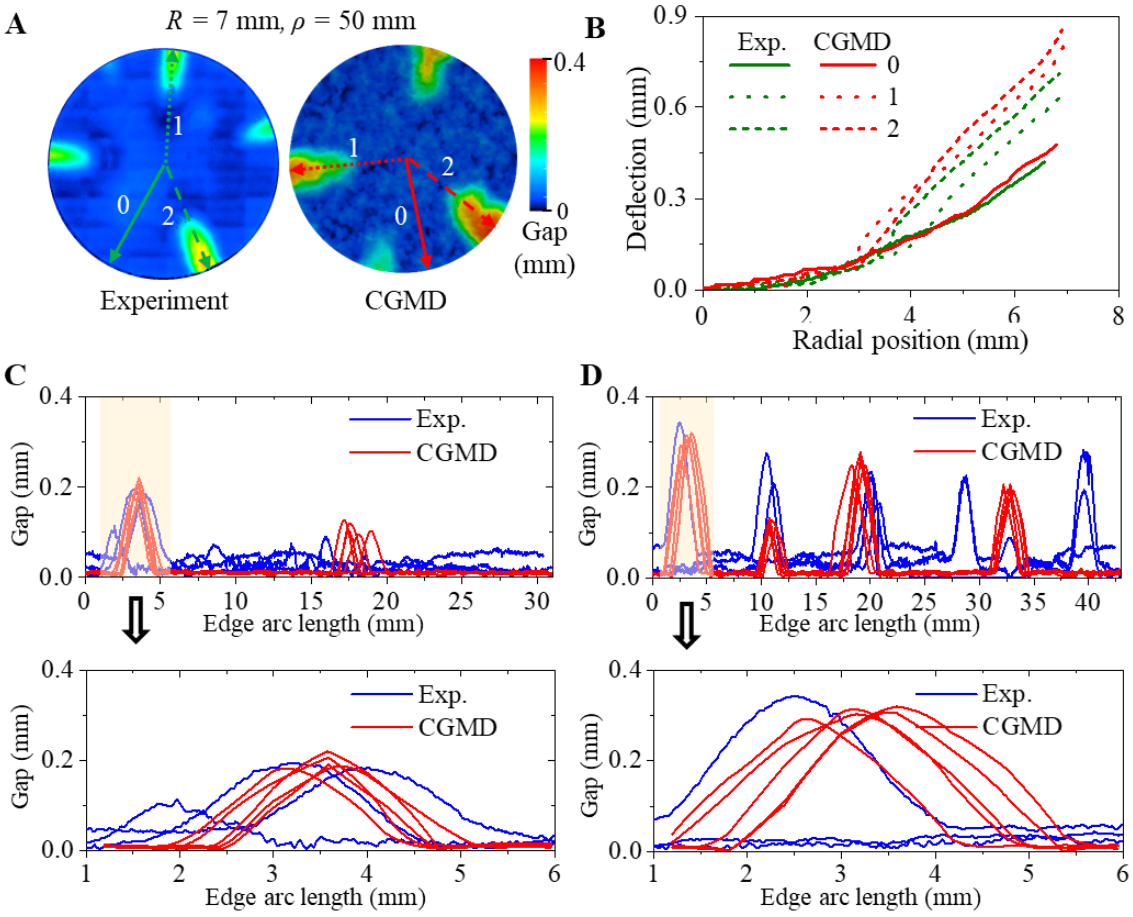


Figure S1. The gap between the sheet and substrate obtained by experiment and CGMD. (**A**) Contour plots of the gap between the sheet and the substrate by optical 3D scan (left) and CGMD simulation (right) for the case of R = 7 mm and ρ = 50 mm. (**B**) Corresponding sheet deflection along the radial direction at fully conformed region (solid curves) and the axes of symmetry of two buckles (dashed and dotted curves). The gap between the sheet and the substrate along the edge of the sheet of five optical 3D scan experiments (blue) and five independent CGMD simulations (red) for the cases of (**C**) R = 5 mm and ρ = 50 mm and (**D**) R = 7 mm and ρ = 50 mm. The zoomed-in profiles of the first blister are shown at the bottom.

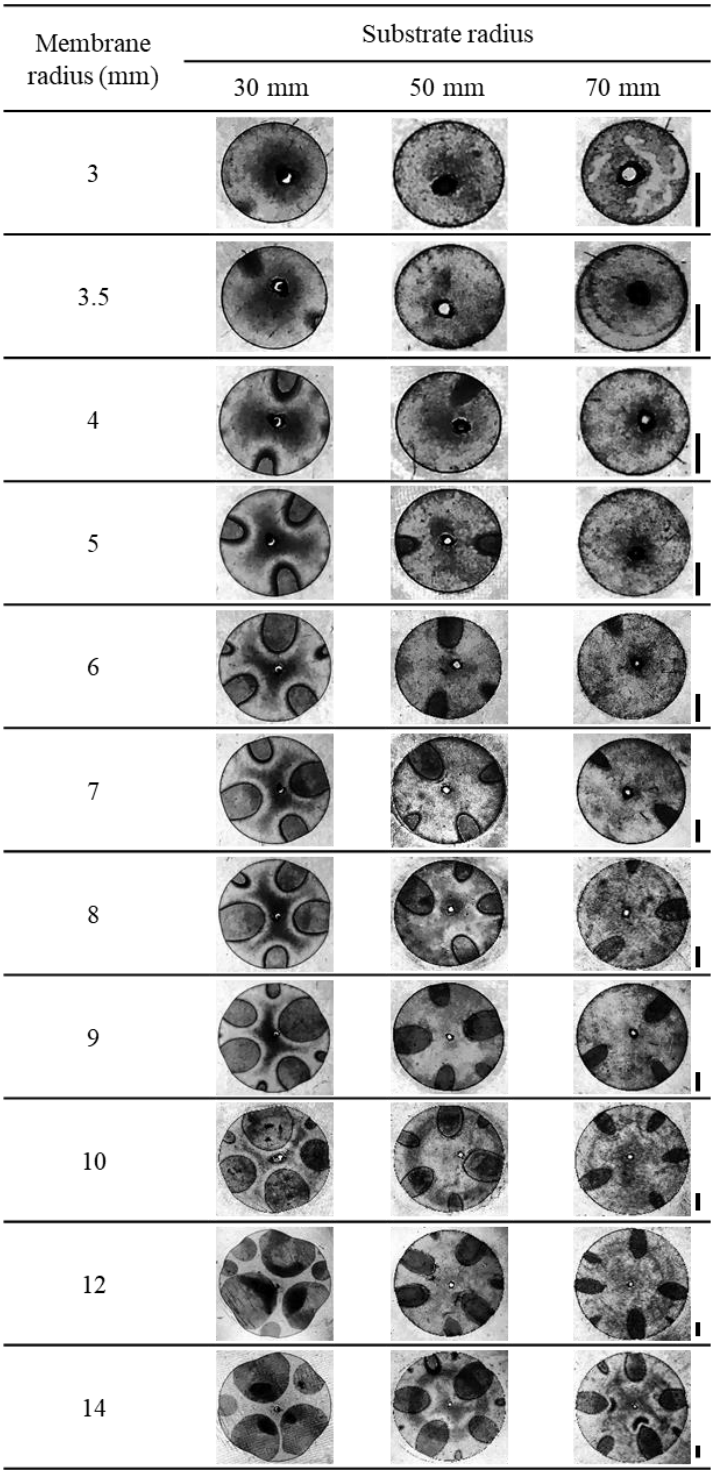


Figure S2. Greyscale images of top-down optical micrographs for different sheet radii and different substrate radii. The scale bars denote 3 mm.

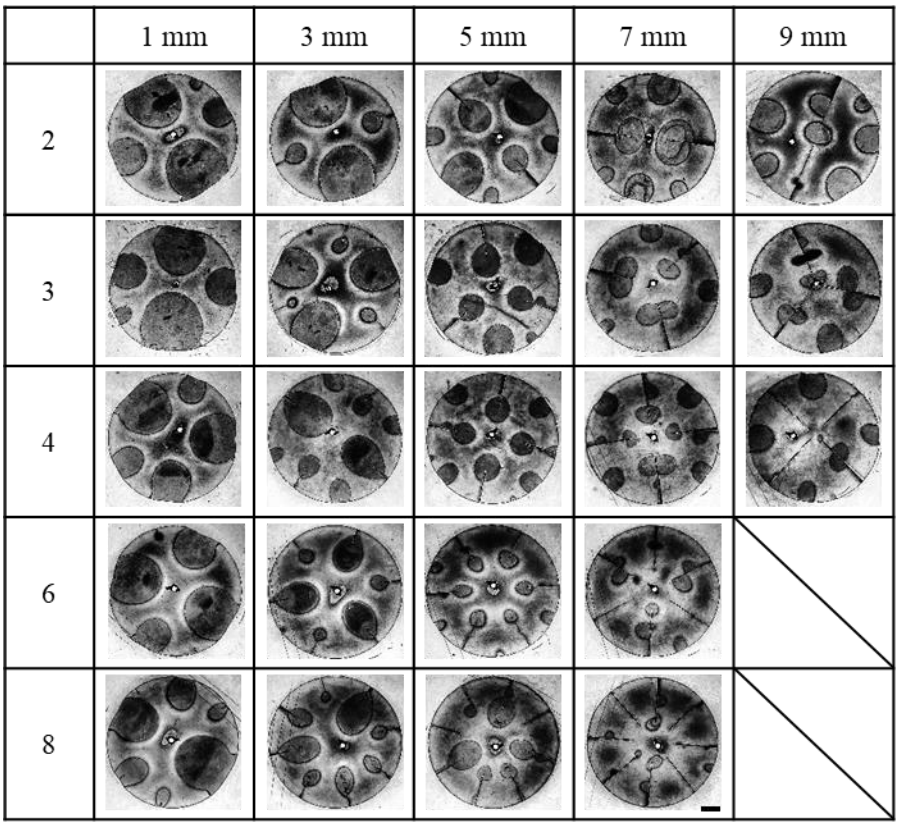


Figure S3. Greyscale images of top-down optical micrographs for different cut lengths and different cut numbers for the case R = 10 mm, ρ = 30 mm. The scale bar denotes 3 mm.

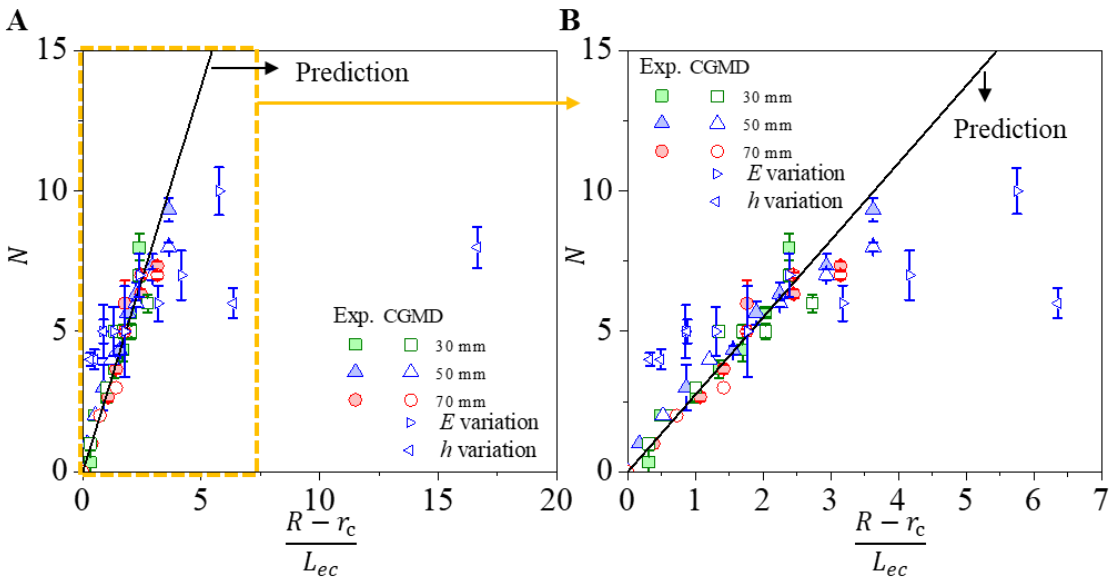


Figure S4. Buckle number for thin sheets with different moduli and thicknesses. (A) Buckle number in experiments (hollow markers), simulations (filled markers), and prediction by Eq. (11) with fitted coefficient based on 3 GPa and 13-μm-thick sheets (solid line). Green, blue, and red denote the substrate radius of 30 mm, 50 mm, and 70 mm, respectively. The triangular markers with a corner pointing to the left denotes simulations with various modulus E and fixed thickness h. The triangular markers with a corner pointing to the right denotes simulations with various thickness h and fixed modulus E. **(B)** An zoom-in view when $(R - r_c) / L_{ec}$ is small.

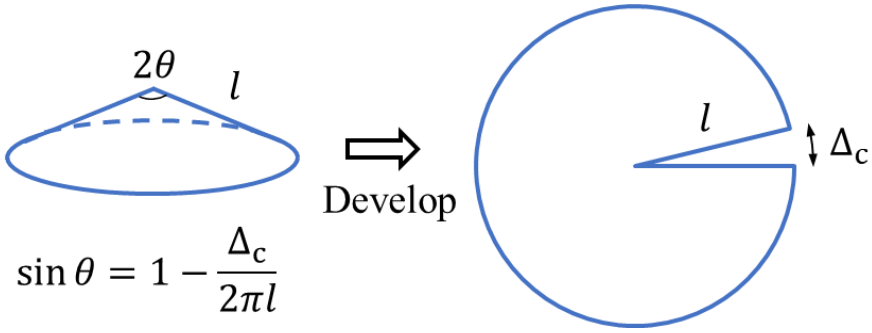


Figure S5. The schematic of a 3D cone developed into a planar circle with a wedge opening.

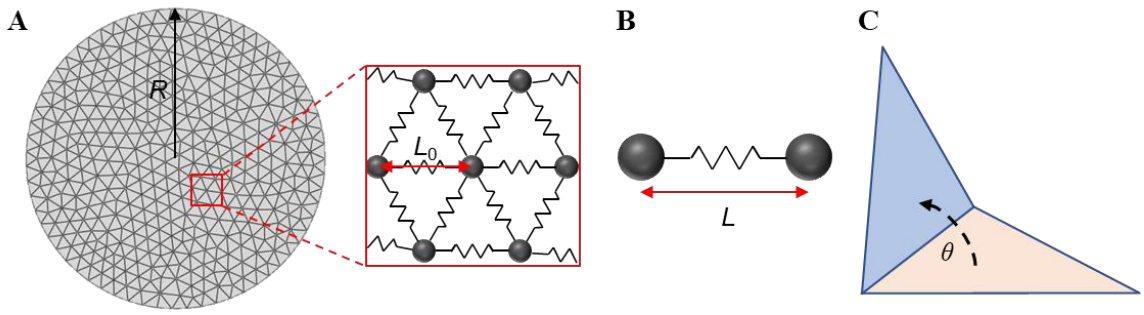


Figure S6. A CGMD model for the thin sheet. (**A**) A circular elastic sheet was discretized into a triangulated network, where particles with mass were located at the lattice points with bonds and elements defined. (**B**) Stretching energy was defined for each bond based on Hooke's Law with an initial bond length of L_0. (**C**) Bending energy was defined for each pair of neighbor elements based on the dihedral angle θ.

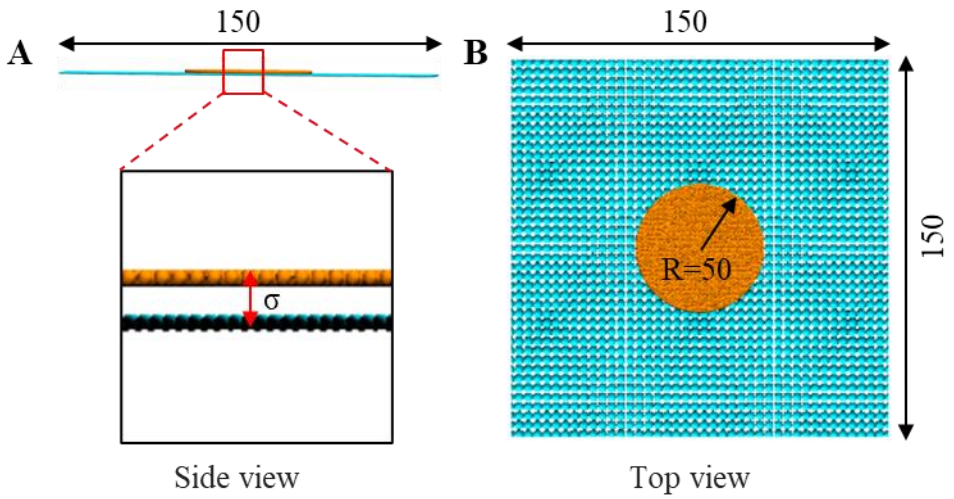


Figure S7. Calibration of interfacial adhesion for the CGMD model. (**A**) side view and (**B**) top view of a 5-mm-radius circular sheet placed on a flat substrate with a distance of σ.

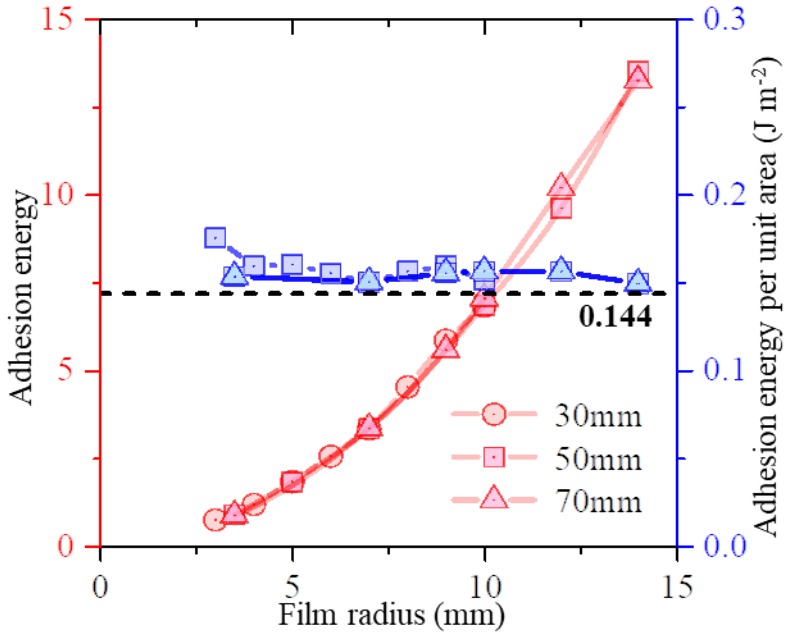


Figure S8. Investigation of adhesion energy for different *R* and *ρ*. The calculated adhesion energy per unit area dominates the well depth of L-J potential for different sheet radii and substrates. The black dashed line defines the adhesion energy in experiments. The red color represents the total adhesion energy between substrate and sheet in simulations. The blue color shows the adhesion energy per unit area between substrate and sheet in simulations, which all are close to the experimental value (0.144 J m^{-2}).

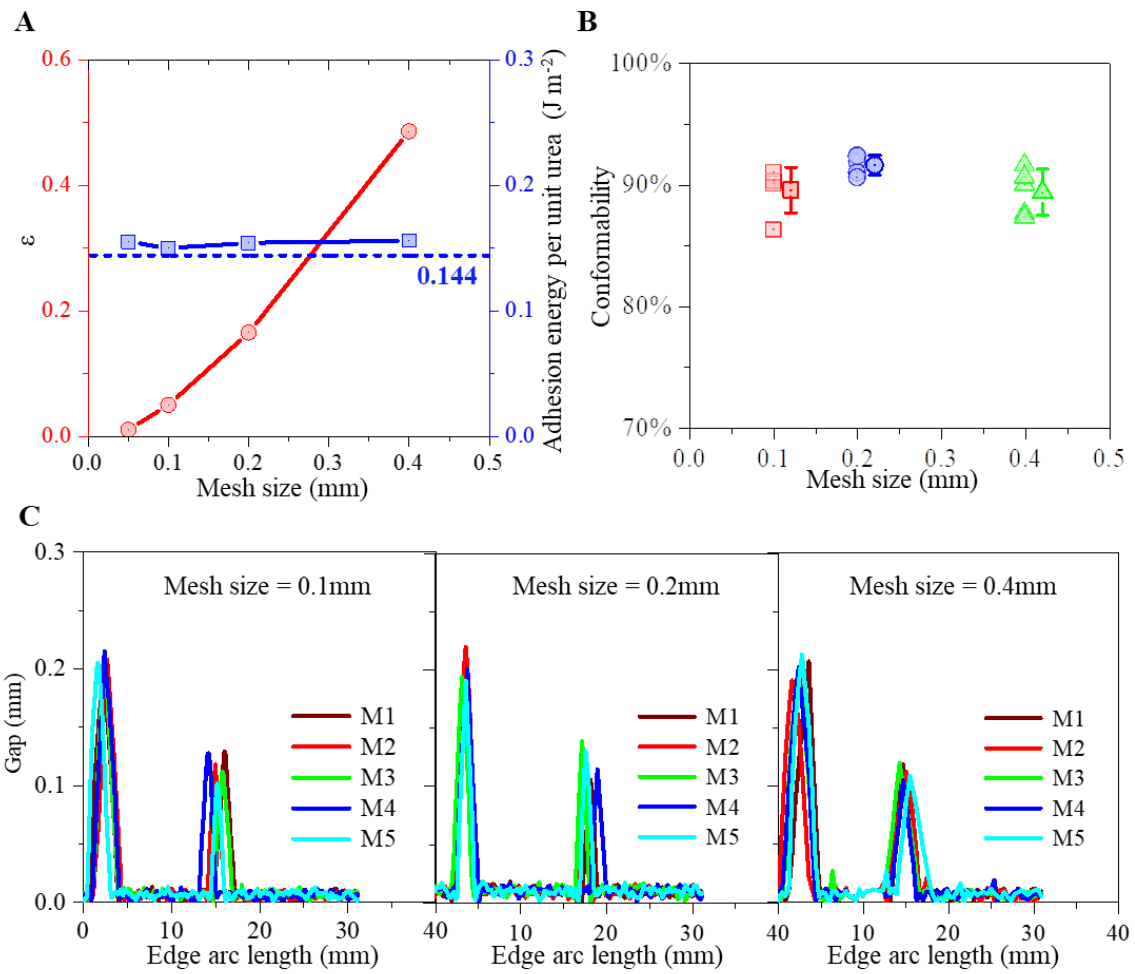


Figure S9. Investigation of proper mesh size in the exemplary case of R = 5 mm and ρ = 50 mm. (**A**) Calibrated well depth of L-J potential and adhesive energy per unit area for different mesh sizes. (**B**) Sheet conformability with different mesh sizes. (**C**) The gap between the sheet and the substrate along the circle boundary for different mesh sizes. Five independent simulations are performed for each case (M1-M5).

Supplementary Movies:

Movie S1. The top-down view of the conforming process of a thin sheet of R = 7 mm, h = 13 μm and E = 3 GPa on a spherical substrate of ρ = 50 mm in CGMD simulation.

Movie S2. The top-down view of the conforming process of a thin sheet of R = 9 mm, h = 52 μm and E = 3 GPa on a spherical substrate of R = 9 mm and ρ = 30 mm in CGMD simulation.

Movie S3. The top-down view of the conforming process of a thin sheet of R = 15 mm, h = 13 μm and E = 3 GPa with 12 curved cuts of 12.9 mm long on a spherical substrate of R = 9 mm and ρ = 30 mm in CGMD simulation.